J|A|C|S ARTICLES

Published on Web 11/12/2009

Ternary Protein Complex of Ferredoxin, Ferredoxin:Thioredoxin Reductase, and Thioredoxin Studied by Paramagnetic NMR Spectroscopy

Xingfu Xu,[†] Peter Schürmann,[‡] Jung-Sung Chung,[§] Mathias A. S. Hass,[†] Sung-Kun Kim,[§,||] Masakazu Hirasawa,[§] Jatindra N. Tripathy,[⊥] David B. Knaff,[§,⊥] and Marcellus Ubbink*[,†]

Leiden Institute of Chemistry, Leiden University, Gorlaeus Laboratories, P.O. Box 9502, 2300 RA Leiden, The Netherlands, Laboratoire de Biologie Moléculaire et Cellulaire, Université de Neuchâtel, Neuchâtel CH-2009, Switzerland, Department of Chemistry and Biochemistry, Texas Tech University, Lubbock, Texas 79409-1061, and Center for Biotechnology and Genomics, Texas Tech University, Lubbock, Texas 79409-3132

Received May 24, 2009; E-mail: m.ubbink@chem.leidenuniv.nl

Abstract: In oxygenic photosynthetic cells, carbon metabolism is regulated by a light-dependent redox signaling pathway through which the light signal is transmitted in the form of electrons via a redox chain comprising ferredoxin (Fd), ferredoxin:thioredoxin reductase (FTR), and thioredoxin (Trx). Trx affects the activity of a variety of enzymes via dithiol oxidation and reduction reactions. FTR reduces an intramolecular disulfide bridge of Trx, and Trx reduction involves a transient cross-link with FTR. NMR spectroscopy was used to investigate the interaction of Fd, FTR, and an m-type Trx. NMR titration experiments indicate that FTR uses distinct sites to bind Fd and Trx simultaneously to form a noncovalent ternary complex. The orientation of Trx-m relative to FTR was determined from the intermolecular paramagnetic broadening caused by the [4Fe-4S] cluster of FTR. Two models of the noncovalent binary complex of FTR/Trx-m based on the paramagnetic distance restraints were obtained. The models suggest that either a modest or major rotational movement of Trx must take place when the noncovalent binary complex proceeds to the covalent complex. This study demonstrates the complementarity of paramagnetic NMR and X-ray diffraction of crystals in the elucidation of dynamics in a transient protein complex.

Introduction

Photosynthesis produces nearly all of the organic carbon in the biosphere. In this process, light not only provides the energy and reducing power (ATP and NADPH) which is required to drive the Calvin cycle but also serves as a regulatory factor for the activity of enzymes involved in carbon assimilation. In oxygenic photosynthetic cells, carbon metabolism is regulated by a light-dependent redox signaling pathway in which ferredoxin:thioredoxin reductase (FTR) plays a central role.[1] The light signal is transmitted in the form of electrons from the chlorophyll-containing thylakoid membrane via a plant type ferredoxin (Fd), FTR, and chloroplastic thioredoxins (including m-type or f-type thioredoxins, abbreviated hereafter as Trx-m and Trx-f), which can activate or deactivate a variety of target enzymes by dithiol−disulfide interchange. Many biochemical and structural investigations have been carried out on the components of this redox cascade.[1−3]

FTR is a disk-shape molecule with a width of about 10 Å across the center. It is an $\alpha\beta$-heterodimer composed of a 13 kDa catalytic subunit that contains a [4Fe-4S] cluster and a variable subunit with sizes ranging from 7 to 13 kDa, depending on the species from which the protein is isolated.[4] The catalytic domain of FTR has seven highly conserved cysteine residues, six of which are organized in two Cys-Pro-Cys (CPC) and one Cys-His-Cys (CHC) motifs. In the FTR from *Synechocystis* sp. PCC 6803, C57 and C87 form the active site disulfide and C55, C74, C76, and C85 serve as ligands of the [4Fe-4S] cluster. In the resting enzyme, a weak interaction between the iron cluster and the disulfide cysteines was suggested on the basis of a Mössbauer spectroscopic study.[5] X-ray diffraction studies on crystals have demonstrated that Fd and Trx-m dock on opposite sides of FTR, enabling the simultaneous interaction of FTR with its electron donor and acceptor.[6] As ferredoxin is a one-electron donor and the reduction of thioredoxin requires two electrons,

[†] Leiden University.
[‡] Université de Neuchâtel.
[§] Department of Chemistry and Biochemistry, Texas Tech University.
[||] Current address: Department of Chemistry and Biochemistry, Baylor University, Waco, Texas 76798.
[⊥] Center for Biotechnology and Genomics, Texas Tech University.

(1) Schürmann, P.; Buchanan, B. B. *Antioxid. Redox Signaling* **2008**, *10*, 1235–1273.
(2) Dai, S. D.; Schwendtmayer, C.; Johansson, K.; Ramaswamy, S.; Schürmann, P.; Eklund, H. *Q. Rev. Biophys.* **2000**, *33*, 67–108.
(3) Dai, S. D.; Johansson, K.; Miginiac-Maslow, M.; Schürmann, P.; Eklund, H. *Photosynth. Res.* **2004**, *79*, 233–248.
(4) Dai, S. D.; Schwendtmayer, C.; Schürmann, P.; Ramaswamy, S.; Eklund, H. *Science* **2000**, *287*, 655–658.
(5) Walters, E. M.; Garcia-Serres, R.; Jarneson, G. N. L.; Glauser, D. A.; Bourquin, F.; Manieri, W.; Schürmann, P.; Johnson, M. K.; Huynh, B. H. *J. Am. Chem. Soc.* **2005**, *127*, 9612–9624.
(6) Dai, S. D.; Friemann, R.; Glauser, D. A.; Bourquin, F.; Manieri, W.; Schürmann, P.; Eklund, H. *Nature* **2007**, *448*, 92–96.

 10.1021/ja904205k CCC: $40.75

the fact that there is only a single Fd-binding site on FTR means that a one-electron-reduced intermediate must participate in the mechanism.

In fact, a two-step reaction mechanism of reduction of Trx by FTR was proposed on the basis of spectroscopic measurements on the enzyme and its *N*-ethylmaleimide (NEM) modified derivative,[5,7,8] and support for the proposed mechanism has been provided by recent X-ray diffraction studies.[6] When the first electron is transferred from Fd to FTR, a one-electron-reduced intermediate is formed. This intermediate contains a unique 5-coordinate cluster Fe in which the sulfur of Cys87 is coordinated to the Fe that interacts with the active-site disulfide and involves an oxidation of the cluster from the EPR-silent 2+ state to a 3+ oxidation state that can be studied by EPR spectroscopy. Rapid freeze−quench experiments have confirmed that the one-electron-reduced FTR indeed is a reaction intermediate.[8] The cleavage of the active site disulfide of FTR that results from these electron transfer reactions converts the exposed Cys57 to the thiol/thiolate state (it is not known whether the sulfur is protonated), enabling it to carry out a nucleophilic attack on the active site disulfide of the oxidized Trx, forming a transient intermolecular disulfide bond with a cysteine on Trx. The second electron, transferred by another molecule of Fd, frees the cluster-ligated cysteine 87 and reduces the $[4Fe\text{-}4S]^{3+}$ form of the cluster to its original $[4Fe\text{-}4S]^{2+}$ oxidation state. The newly released cysteine 87 attacks and cleaves the intermolecular disulfide bond between FTR and Trx, completing the formation of reduced Trx and re-forming the disulfide form of the active-site FTR cysteine pair. Thus, the role of the [4Fe-4S] cluster involves more than the mere catalysis of electron transfer from Fd to Trx. The five-coordinated cluster stabilizes the one-electron-reduced intermediate, enabling the reaction between two successive one-electron donors (Fd) and one two-electron acceptor (Trx) to occur without the release of reactive intermediates. In the recent X-ray diffraction study, crystal structures of trapped intermediate states including the cross-linked binary complexes of FTR with monocysteine Trx mutants and the ternary complex of Fd with cross-linked FTR/Trx were obtained, providing convincing evidence for the proposed reaction mechanism. These structures could be obtained because a mutant Trx was used in which one active site Cys was mutated to Ser. As a consequence, the second reaction step was impaired, trapping the intermediate.

In the present study, two-dimensional NMR spectroscopy was used to study the interaction of Fd, FTR, and Trx-m. NMR titration experiments indicate that FTR can bind to Fd and Trx-m simultaneously to form a noncovalent ternary complex in solution. Utilizing the paramagnetism of the $[4Fe\text{-}4S]^{2+}$ cluster of FTR, the binding site for FTR on Trx-m in the noncovalent complex was mapped. The interaction interface on Trx-m for FTR includes the active site WCGPC motif and neighboring residues. The intermolecular paramagnetic effects also provide information about the relative orientations of Trx and FTR within the noncovalent complex. A comparison between two solution models of the noncovalent FTR/Trx-m binary complex based on the paramagnetic restraints and the crystal structure of the cross-linked complex suggests that rotational movement is required for the noncovalent complex to proceed to the cross-linked intermediate.

Experimental Section

Protein Production and Purification. Recombinant forms of *Synechocystis* sp. PCC 6803 Fd and FTR were produced in *Escherichia coli* and purified as described previously.[9] For the production of ^{15}N thioredoxin, a culture of *E. coli* BL21 (DE3) harboring a plasmid derived from pET28b and encoding spinach Trx-m was incubated in minimal medium containing $^{15}NH_4Cl$ (0.5 g/L) and kanamycin (50 mg/L) at 37 °C until the OD_{600} was 0.6. Then, IPTG (isopropyl β-D-thiogalactopyranoside) was added to a final concentration of 1 mM, and incubation was continued for 16 h in M9 medium at 30 °C. Cells were harvested by centrifugation, resuspended in 50 mM sodium phosphate buffer (pH 8.0) containing 200 mM NaCl, passed five times through a French press at 18 000 psi, and centrifuged at 50 000 rpm for 1 h. The supernatant was filtered through a 0.45 μm pore-size membrane and applied to a Ni^{2+} affinity column (HisTrap Chelating HP, obtained from Amersham Bioscience) incorporated into a BioCAD perfusion chromatography system (PerSeptive BioSciences). The column was washed with 50 mM sodium phosphate buffer (pH 8.0) containing 500 mM NaCl (buffer A), supplemented with 10 mM imidazole, followed by a wash with buffer A containing 125 mM imidazole. The His-tagged protein was then eluted with buffer A containing 250 mM imidazole. The elution buffer was exchanged for 50 mM sodium phosphate buffer by ultrafiltration using the Amicon YM10 membrane. The concentration of Trx-m was determined from the predicted absorbance at 280 nm (ε = 22.2 mM^{-1} cm^{-1}). The protein was >95% pure based on SDS−PAGE. The yield was 3 mg/L of culture.

NMR Measurements. Samples for NMR spectroscopy contained 20 mM sodium phosphate buffer, pH 6.5, and 5% D_2O. NMR experiments were conducted using a Bruker DMX 600 spectrometer equipped with TCI-Z-GRAD cryoprobe. For ^{15}N-labeled oxidized Trx-m, the backbone amide assignments were obtained using a $^1H-^{15}N$ HSQC spectrum and three-dimensional $^1H-^{15}N$ TOCSY−HSQC and $^1H-^{15}N$ NOESY−HSQC spectra measured at 298 K. NMR data-processing was performed using AZARA (http://www.bio.cam.ac.uk/pub/azara) and the spectra were analyzed in Ansig-for-Windows.[10]

On the basis of the available proton assignments of spinach Trx-m,[11] most of ^1H and ^{15}N resonances of backbone NH groups were assigned except for some overlapping cross-peaks. Residues without backbone amide assignment are E4, A5, E8, V9, S24, W36, G38, and I77. The indole side chain NH groups of W33 and W36 were assigned on the basis of previous proton assignments.

In titration experiments, $^1H-^{15}N$ HSQC spectra were recorded on samples of 0.2 mM ^{15}N Trx-m into which unlabeled FTR was titrated. To observe formation of the ternary complex, a HSQC spectrum was first recorded on a sample of 0.2 mM ^{15}N Trx-m and then aliquots of a solution of 2 mM unlabeled FTR were titrated into ^{15}N Trx-m to a molar ratio of 1:1. Finally, microliter aliquots of highly concentrated ^{15}N-labeled Fd were added to the binary FTR/Trx-m complex to a molar ratio of 3.2 (Fd:FTR).

^{15}N R_1 and CPMG R_2 measurements at 14.1 T were made on 0.3 mM ^{15}N labeled Fd, and on ^{15}N labeled Fd in the presence of Trx-m (Fd:Trx-m 1:1) and in the presence of both Trx and FTR (Fd:Trx-m:FTR 1:1:1). Samples contained 20 mM sodium phosphate buffer, pH 6.5, in 95% H_2O and 5% D_2O, and the measurements were carried out at 298 K. Published NMR pulse

(7) Staples, C. R.; Ameyibor, E.; Fu, W. G.; Gardet-Salvi, L.; Stritt-Etter, A. L.; Schürmann, P.; Knaff, D. B.; Johnson, M. K. *Biochemistry* **1996**, *35*, 11425–11434.
(8) Staples, C. R.; Gaymard, E.; Stritt-Etter, A. L.; Telser, J.; Hoffman, B. M.; Schürmann, P.; Knaff, D. B.; Johnson, M. K. *Biochemistry* **1998**, *37*, 4612–4620.
(9) Xu, X. F.; Kim, S. K.; Schürmann, P.; Hirasawa, M.; Tripathy, J. N.; Smith, J.; Knaff, D. B.; Ubbink, M. *FEBS Lett.* **2006**, *580*, 6714–6720.
(10) Helgstrand, M.; Kraulis, P.; Allard, P.; Härd, T. *J. Biomol. NMR* **2000**, *18*, 329–336.
(11) Neira, J. L.; Gonzalez, C.; Toiron, C.; dePrat-Gay, G.; Rico, M. *Biochemistry* **2001**, *40*, 15246–15256.

programs[12] were used. Four to seven 2D planes were recorded for each relaxation measurement with different relaxation delays ranging from 10−1500 ms and 0−180 ms for the R_1 and R_2 measurements, respectively.

The peak intensities were evaluated for 73 signals in the case of free Fd and Fd in the presence of Trx-m. For Fd in the presence of both FTR and Trx-m, only 36 signals were evaluated, because of the lower signal-to-noise ratio. R_2 and R_1 rates were obtained from a single-exponential fit of the intensity versus the relaxation delay. The average R_2/R_1 was trimmed 15% to avoid biases from chemical exchange on the microsecond−millisecond time scale or slow dynamics on the picosecond−nanosecond time scale. Furthermore, the average was weighted by the standard error of the individual R_2/R_1 ratios. Rotational correlation times were calculated from the trimmed weighted average R_2/R_1 value using equations for R_1 and R_2.[13,14]

Docking and Modeling. Trx-m residues were assigned to three categories on the basis of the paramagnetic relaxation enhancement (PRE) that they experienced. Class I comprised the residues of which the resonances disappeared early during the titration, indicating large PRE. Analogously, those with a resonance broadening later in the titration were assigned to class II. The remaining residues formed class III. The paramagnetic effects were translated into loose distance restraints. For calibration of these distances, effects observed in an earlier study for two residues, Cys39 and Ala40, of Ga-substituted Fd bound to FTR were used.[9] The resonances of these residues disappeared during a similar NMR titration and are known to be 15−18 Å away from the [4Fe-4S] cluster in the Fd:FTR complex.[6] For class I, the distance between the geometric center of the [4Fe-4S] cluster and the amide nitrogen was restrained with a lower and upper bound of 10 and 15 Å, respectively. For class II, these limits were 10 and 20 Å and for class III 18 and 40 Å.

Docking calculations were carried out with the programs BIGGER (*bi*molecular complex *g*eneration with *g*lobal *e*valuation and *r*anking)[15] and HADDOCK (*h*igh *a*mbiguity *d*riven biomolecular *dock*ing).[16] Structure coordinates of free FTR (PDB access code 1DJ7) and Trx-m (1FB6)[17] were used as input for the docking. In BIGGER, FTR was the target and Trx-m the probe for searching for the possible solutions of the complex geometry. For each orientation of two proteins, optimal surface matching was first achieved by translational shifting of the probe matrix relative to the target matrix. The probe was rotated by 15° for each step until a complete search was performed. All solutions containing unrealistic backbone steric clashes were discarded, but the side chains of residues Arg, Lys, Asp, Glu, and Met were allowed to penetrate over the flexible surface of the other proteins as long as there was no unrealistic penetration. The ensemble of 5000 saved model structures was used for the subsequent cluster analysis. The experimental distance restraints derived from intermolecular PREs were used to filter out the structures that were in agreement with the NMR data.

The residues C57 of FTR and A34, W36, and I80 of Trx-m are solvent accessible in free proteins and were defined as active residues for docking in HADDOCK. The unambiguous intermolecular restraints derived from PRE effects were used in all stages of docking. The FeS cluster could not be used for the PRE distance restraints for technical reasons, so the S^{γ} of FTR C87 was used instead. Distance restraints with lower and upper bounds of 5 and 13 Å between Trx-m amide nitrogens and the C87 S^{γ} atom were used for class I residues. For class II residues, 5 and 15 Å were employed as lower and upper bounds, respectively. An extra set of distant restraints was used to fix the orientation between two subunits of FTR. During the first stage of calculations, 1000 rigid-body docking models were generated. The 200 lowest energy complexes were selected for semiflexible simulated annealing with fixed backbone conformations. The 200 lowest energy models were then refined in water and clustered using a 2.5 Å rmsd cutoff.

Results

Binary Complex of FTR and Trx. To characterize the Trx/FTR complex in solution, a titration experiment was performed by recording $^{15}N-^{1}H$ HSQC spectra of Trx-m upon addition of small aliquots of unlabeled FTR. Changes in NMR signal intensities and chemical shifts were monitored. During the first four titration points, to a Trx:FTR ratio of 1:0.27, some resonances showed fast intensity decrease and significant line broadening. At the seventh titration point, with a Trx:FTR ratio of 1:0.54, many peaks had disappeared, whereas some resonances show small chemical shift changes. At the final titration point, the chemical shift changes of those residues were saturated, suggesting that all the Trx-m was in a bound state in the presence of an excess of FTR. Careful analysis of the perturbed chemical shifts indicates that the peak positions are not proportional to the fraction of bound Trx, but rather that the resonances show slow-intermediate exchange behavior, i.e., a decrease of the signals of free Trx and concomitant increase of those of the bound state. This is illustrated by the resonances of S94 (Figure 1), from which the exchange rate constant could be deduced to be $\ll 150\ s^{-1}$. For those residues that disappeared during the titration, no cross-peaks reappeared for the last titration point representing the fully bound state of Trx/FTR (Figure 1). This phenomenon can be attributed to the combined broadening due to the complex formation, which increases the rotational correlation time of Trx, and thus the line width, and intermolecular PRE originating from the iron sulfur cluster of FTR. The broadening effects cannot be due to exchange broadening, because the exchange rate constant is too low to cause large broadening and the resonances of the bound form would be expected to become visible during the titration.

Interaction Mapping Based on Intermolecular PRE. Residues of Trx-m experiencing intermolecular PRE upon complex formation with FTR were mapped onto the protein surface of Trx-m to illustrate the binding site (Figure 2). The residues experiencing the paramagnetic effect can be classified into two groups. Those in class I, which includes residues F32, A34, C37, and I80, show a fast intensity drop during the first four titration points, suggesting that their backbone amides get close to the cluster and experience strong paramagnetism in the complex. The cross-peak of indole side chain NH^{ε} group of W36, an amino acid that is at the core of the interaction interface with FTR, has completely disappeared after the third titration point. Class II residues, experiencing a lesser degree of PRE, are located around the core interface, including the charged residues K41, D66, and R78; polar residues T65, T73, and S79; and the nonpolar residues A68, G70, I71, A72, and V83. The interaction interface of Trx-m in the complex FTR/Trx-m includes the typical WCGPC motif and peripheral residues.

Orientation of Trx-m in the Complex with FTR. PRE results from the magnetic dipolar interaction between a nucleus and

(12) Farrow, N. A.; Muhandiram, R.; Singer, A. U.; Pascal, S. M.; Kay, C. M.; Gish, G.; Shoelson, S. E.; Pawson, T.; Forman-Kay, J. D.; Kay, L. E. *Biochemistry* **1994**, *33*, 5984–6003.
(13) Abragam, A. *Principles of Nuclear Magnetism*; Claredon Press: Oxford, 1961.
(14) Cavanagh, J.; Fairbrother, W.; Palmer, A. G., III; Skelton, N. J. *Protein NMR Spectroscopy: Principles and Practice*; Academic Press Inc.: San Diego, CA, 2006.
(15) Palma, P. N.; Krippahl, L.; Wampler, J. E.; Moura, J. J. G. *Proteins−Struct. Funct. Genet.* **2000**, *39*, 372–384.
(16) Dominguez, C.; Boelens, R.; Bonvin, A. M. J. J. *J. Am. Chem. Soc.* **2003**, *125*, 1731–1737.
(17) Capitani, G.; Markovic-Housley, Z.; DelVal, G.; Morris, M.; Jansonius, J. N.; Schürmann, P. *J. Mol. Biol.* **2000**, *302*, 135–154.

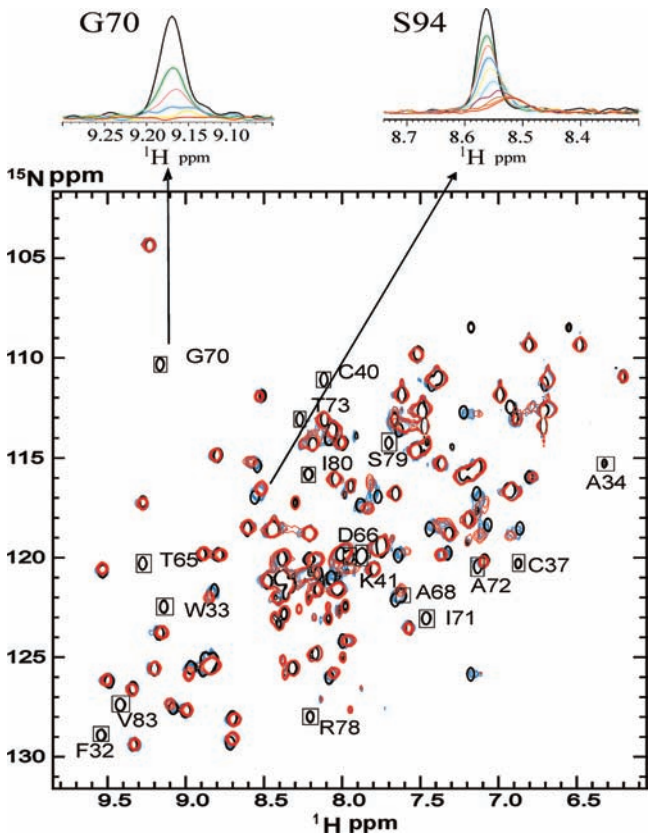

Figure 1. Overlay of ^{1}H−^{15}N HSQC spectra of ^{15}N Trx-m in the titration experiments: black, Free Trx-m; cyan, Trx-m/FTR at a ratio of 1:0.54; red, ratio 1:1.26. The resonances of the residues experiencing a PRE effect in FTR/Trx-m complex are labeled. The cross sections along the F2 dimension through the ^{1}H^N resonances of residues G70 and S94 at different titration points are shown in the top panel. The slices show the ratios of FTR/Trx-m of 0, 0.09, 0.18, 0.27, 0.36, 0.54, 0.72, 0.99, 1.17, and 1.26 in black, green, pink, blue, yellow, cyan, magenta, brown, orange, and red, respectively.

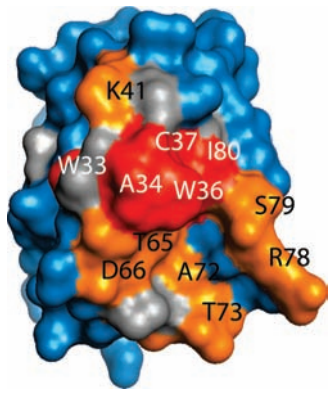

Figure 2. Surface representation of Trx-m (PDB access code 1FB6) showing the interaction area in the noncovalent FTR/Trx-m complex. Residues experiencing strong and weak paramagnetic effects of [4Fe-4S] are in red and orange, respectively. Residues that experience no paramagnetic effect are in blue. Residues without assignment are in gray.

the unpaired electrons in a metal center or stable radical. The magnitude of PRE is proportional to the reciprocal sixth power of the distance between the nucleus and the metal center. Effects can be observed over large distances because of the large magnetic moment of an unpaired electron, and these effects can be employed for structure calculation. Taking advantage of this phenomenon, the paramagnetic broadening of Trx-m residues was converted into distance restraints to guide docking calculations of Trx-m on FTR.

The [4Fe-4S] cluster of FTR in the $[4Fe\text{-}4S]^{2+}$ oxidation state found in the resting enzyme contains two Fe^{3+} and Fe^{2+}. The ground state is $S = 0$, but magnetically active states are populated at room temperature. Previously, a diamagnetic structural analog of Fd with a single Ga ion replacing the [2Fe-2S] cluster found in native Fd was used to determine the complete interaction site on Fd in the FTR/Fd complex in solution. Two residues (C39 and A40) of Fd were suggested to sense the intermolecular PRE effect in the FTR/Fd complex.[9] The distances from the amides of C39 and A40 in Fd to the [4Fe-4S] cluster of FTR in the crystal structure of the Fd/FTR complex were used to calibrate the strength of the paramagnetism of [4Fe-4S] iron sulfur cluster. The Trx-m residues were assigned to three classes associated with loose distance restraints, on the basis of the observed PRE effects and this calibration. Lower and upper bounds of 10 and 15 Å, respectively, of the distance between the amide nitrogen and the [4Fe-4S] cluster center were applied to the residues with strong PRE effects (class I). For class II residues, these limits were 10 and 20 Å and for the residues without intermolecular PRE effects (class II) 18 and 40 Å were used.

Docking calculations to obtain the possible conformations of the noncovalent binary complex of FTR/Trx-m were performed using two programs, BIGGER and HADDOCK. With BIGGER, an initial set of orientations of Trx-m was selected during a systematic search of the conformational space, scored on the basis of geometric complementarities and electrostatic interactions. All solutions were then scored and clustered using the distance restraints derived from the PRE data (see Experimental Section). The geometrical centers of Trx-m are shown for these orientations as yellow spheres in Figure 3A. Interestingly, two clusters are found on opposite sides of FTR. The cluster on the left in Figure 3A is in fact the side where Fd binds. This side cannot be the Trx binding site because it places Trx far from the FTR active site Cys57, which forms the transient intermolecular disulfide bridge with Trx. The 10 best solutions are shown as the small red cluster on the right of FTR in Figure 3A. In these conformations, the active site residues of Trx-m are close to the active site disulfide of FTR and the short helix formed by G70-T73 is docked into the concave region formed by the catalytic and variable subunits of FTR (Figure 3B). The orientation of Trx-m deviates significantly from that observed for the cross-linked complex, as will be discussed later.

HADDOCK uses a somewhat different approach, in which docking criteria (van der Waals and electrostatic interactions) are combined with experimental restraints throughout the docking procedure. After obtaining the rigid body complexes, a second stage in the simulation includes flexibility of the side chains in the interface to remove bad contacts. Interestingly, the two top clusters from the HADDOCK simulations resemble the orientations of Trx-m in the cross-linked complex and in the structure of the complex found with BIGGER (Figure 3, panels C and D). This result indicates that both orientations have favorable binding properties with large, negative electrostatic and van der Waals energy terms (Supporting Information, Table S-1). Although the experimental restraints are important in the initial stages of the docking, toward the end, the restraint energies are small in comparison to the electrostatic and van der Waals terms, implying that the restraints contribute little to the fine-tuning of the orientation of Trx-m in the complex. A

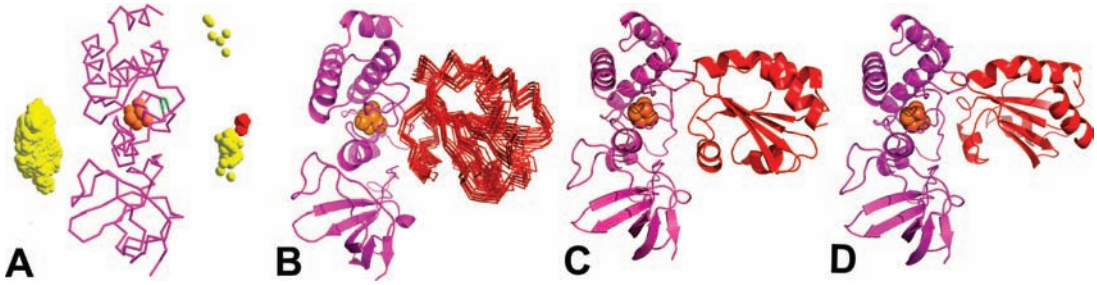

Figure 3. Docking of FTR/Trx-m complex. (A) BIGGER docking solutions of the FTR/Trx-m complex. FTR is indicated by a purple C^{α} trace, the [4Fe-4S] cluster is shown as orange spheres, and C57 and C87 are in green. The geometrical centers of Trx-m of 5000 solutions are represented by yellow spheres. The top 10 solutions in BIGGER docking based on PRE restraints scoring are in red. (B) The BIGGER ensemble of top 10 structures with FTR superimposed. Trx-m structures are shown as C^{α} traces and FTR is shown as ribbons. (C, D) Representative structure of HADDOCK cluster 1 (C) and 2 (D). Trx-m and FTR are shown as red and purple ribbons, respectively.

Table 1. Relaxation Analysis of Fd in Complex with FTR[a]

sample[b]	$\langle R_2 \rangle$ (s^{-1})	$\langle R_1 \rangle$ (s^{-1})	$\langle R_2/R_1 \rangle_{trim}$[c]	τ_{rot}[d] (ns)	M_r[e] (kDa)	M (kDa)
Fd	7.39 ± 0.07	2.10 ± 0.02	3.55 ± 0.01	5.02 ± 0.01	10.5 ± 0.1	11
Fd + Trx-m	7.99 ± 0.08	2.01 ± 0.01	3.93 ± 0.15	5.40 ± 0.15	11.5 ± 0.4	25
Fd + FTR[f]	27.8 ± 0.3	1.05 ± 0.07	26.5 ± 0.3	14.5 ± 0.5	36.8 ± 1.4	32
Fd + Trx-m + FTR	41.6 ± 0.3	1.06 ± 0.04	31.0 ± 2.0	17.7 ± 0.6	46 ± 2	46

[a] The average ^{15}N relaxation parameters R_1 and R_2 at 14 T, rotational correlation times τ_{rot}, effective molecular mass M_r, and theoretical molecular mass M of the complex are reported for oxidized Fd from *Synechocystis* sp PCC 6803, and for Fd in the presence of Trx-m and FTR at 298 K and pH 6.5. [b] All protein concentration ratios are 1:1. [c] 15% trimmed average. [d] Calculated from $\langle R_2/R_1 \rangle_{trim}$ assuming an isotropic rotational diffusion tensor. [e] Effective molecular mass calculated from τ_{rot} using Stokes equation, and assuming the protein or protein complex is a sphere coated with a 3.2 Å hydration shell tightly bound to the protein surface. [f] The measurement was conducted on a sample with a concentration of 1.4 mM at 293K and the τ_{rot} at 298K was converted based on an empirical equation.[18]

detailed comparison between the modeling results and the cross-linked complex is given in the Discussion.

Ternary Complex Formation. To establish whether a noncovalent ternary complex between Trx-m, FTR, and Fd is formed in solution, several NMR experiments were performed. When unlabeled Trx-m was titrated into a solution of ^{15}N-labeled Fd to a 1:1 ratio, no significant chemical shift changes were found for Fd (Supporting Information, Table S-2). The rotational correlation time of Fd, which was determined by ^{15}N relaxation analysis, increases only slightly from 5.0 to 5.4 ns (Table 1), showing that there is no specific interaction between Fd and Trx-m. Upon addition of unlabeled FTR to this equimolar mixture of Trx and Fd, many Fd peaks shift significantly, all signals broaden, and several signals disappear in the HSQC spectrum. These changes agree with those reported for the binary complex of FTR and Fd[9] (Supporting Information, Figure S-1 and Table S-2). Furthermore, the rotational correlation time of Fd increases to 18 ns. This correlation time corresponds to an effective molecular mass of 46 kDa, which is equal to the expected mass of the ternary complex of Fd, FTR, and Trx (Table 1).

A second titration experiment using ^{15}N-labeled Trx-m, ^{15}N-labeled Fd, and unlabeled FTR was carried out. When FTR was titrated into the ^{15}N-labeled Trx-m to a molar ratio of 1.0, the complex formation between FTR and Trx-m occurred, as indicated by the line broadening and small chemical shift changes of resonances of Trx-m as described above. Then, ^{15}N-labeled Fd was titrated into the binary complex. Although the introduction of the second ^{15}N-labeled sample resulted in a crowded HSQC spectrum, a well-dispersed region of the spectrum could be used to monitor the association or dissociation of the components. The intensity change and chemical shift change pattern of residue 93 of Fd are the same as those observed in the binary complex of FTR and Fd,[9] which indicates the association of Fd with FTR. No further chemical shift changes of residues of Trx-m are observed when Fd is titrated into the binary complex, suggesting that Trx-m remains bound and unperturbed when Fd associates with FTR (Figure 4). It is concluded that a noncovalent ternary complex Fd:FTR:Trx-m is formed in solution in which Fd and Trx-m use distinct interfaces to interact with FTR.

Discussion

Comparison of Noncovalent Complex with the Cross-Linked Binary Complex of FTR/Trx-m. The distances between the amide nitrogens and the FTR [4Fe-4S] cluster were measured for the models of the noncovalent complexes and the crystal structure of the cross-linked reaction intermediate FTR/Trx-mC40S. In Figure 5 these distances are compared with the NMR-derived distance restraints. The upper and lower bounds are indicated by the blue and red lines, respectively. For residues affected by PRE, 10 Å was used as lower bound to avoid the steric clashes. Upper bounds of 15 and 20 Å were used for strongly and weakly affected residues, respectively. For residues without significant PRE effect, 18 Å was used as the lower bound. The noncovalent BIGGER complex was obtained by scoring on these criteria and therefore can be expected to fit the NMR-based restraints well (Figure 5A). In contrast, the cross-linked structure does not satisfy all restraints. The major violation is for the residues G70-T73, which are located far (>20 Å) from the iron sulfur cluster in the cross-linked FTR/Trx-m. In panel B of Figure 5, the same analysis is shown for the two top clusters of structures obtained with HADDOCK. Both clusters show good agreement with the NMR-derived distances. One cluster has been rotated relative to the other around the α-helix formed by Trx-m residues 42−54, leaving the 30−40 region in about the same place while turning the 62−82 region

(18) de la Torre, J. G.; Huertas, M. L.; Carrasco, B. *J. Magn. Reson.* **2000**, *147*, 138–146.

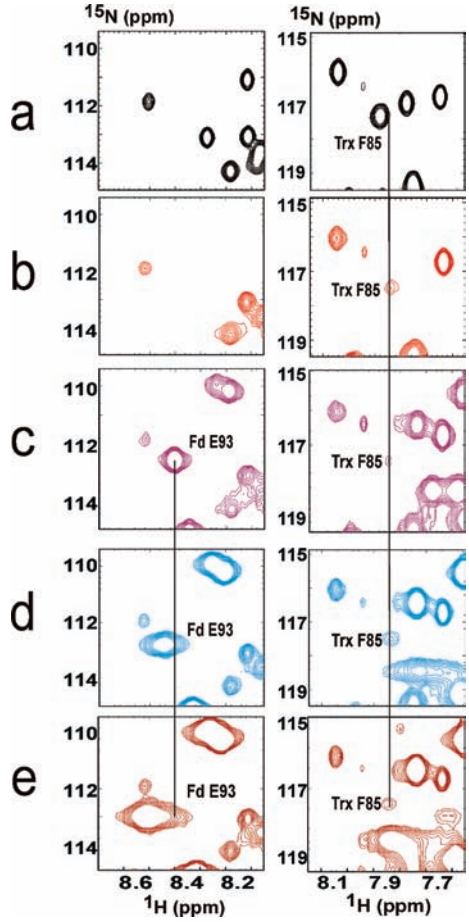

Figure 4. Formation of a noncovalent ternary complex of Fd, FTR, and Trx-m, monitored in a HSQC titration experiment. The association of FTR with Trx-m was demonstrated by a chemical shift change and line broadening of the resonance of Trx-m F85. The association of Fd with FTR was followed by observing the behavior of the resonance of Fd E93. ^{15}N-^{1}H HSQC of (a) free ^{15}N Trx-m, (b) ^{15}N-Trx:FTR (1:1), (c) ^{15}N-Trx:FTR:^{15}Fd (1:1:1), (d) ^{15}N-Trx:FTR:^{15}N-Fd (1:1:2), and (e) ^{15}N-Trx:FTR:^{15}N-Fd (1:1:3.2). The vertical lines indicate the resonance positions for the bound state of Fd E93 (left) and Trx-m F85 (right).

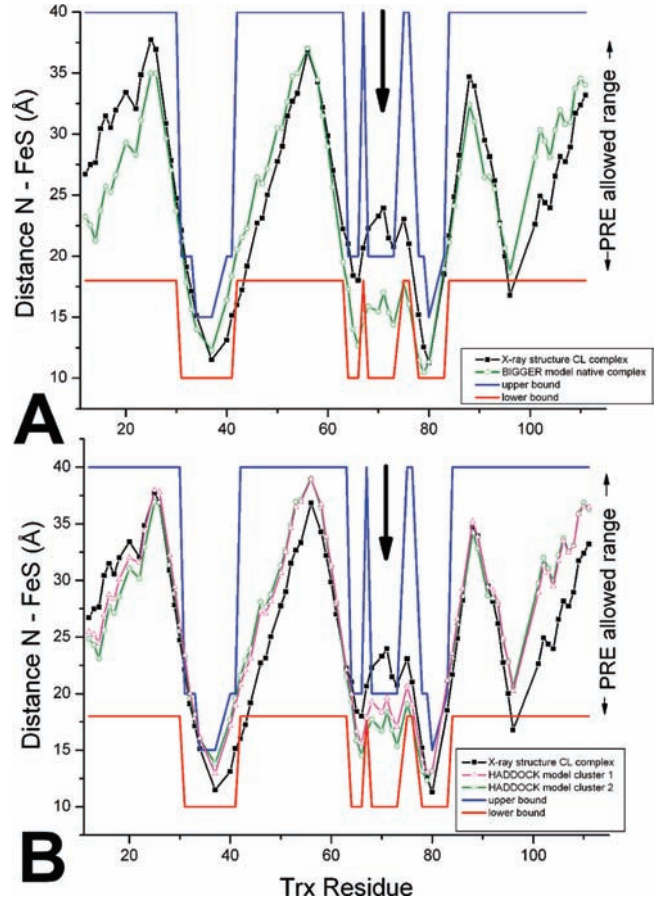

Figure 5. Comparison of cross-linked and noncovalent FTR/Trx-m models with paramagnetic restraints. Distances are shown between amide nitrogens of Trx-m and the iron−sulfur center in the cross-linked complex as a black line and squares (A, B), the noncovalent FTR/Trx-m BIGGER model as a green line and circles (A), the HADDOCK cluster 1 model as a pink line and triangles (B) and the HADDOCK cluster 2 model as a green line and circles (B). The blue and red lines indicate the upper and lower distance bounds, respectively, derived from PRE effects. The G70−T73 region, exhibiting a discrepancy with the distance restraints in the cross-linked FTR/Trx-m, is marked with an arrow.

to the other side of the interface (Figure 6), but at about equal distance from the FeS cluster. It is concluded that on the basis of the NMR data the two models cannot be distinguished, because significant PRE effects are observed only for these regions. HADDOCK cluster 2 resembles the BIGGER solution (Figure 6B), whereas cluster 1 is closer to the cross-linked complex (Figure 6C).

In the BIGGER structure and HADDOCK cluster 2, Trx-m has a similar interface for docking to FTR as in the cross-linked complex. In the noncovalent complexes, the active site cysteine C32 of Trx-m can get close to the C57 of FTR, whereas these two residues are disulfide-bonded in the cross-linked complex. In the noncovalent complexes, however, the short helix G70−T73 of Trx-m docks partially into a concave region formed by the two subunits of FTR, whereas in the crystal structure of the cross-linked complex, the G70−T73 region of Trx-m has a direct contact with a loop (residue 58−61) in the catalytic subunit of FTR. The comparison of these two models suggests that a rotational movement of about 50° relative to FTR would be necessary for Trx-m to proceed from the noncovalent to the cross-linked complex. The second HADDOCK cluster has a Trx-m orientation that is closer to the cross-linked structure (Figure 6C) but is slightly rotated around a vector roughly formed by the Trx-m residues E25 and N88 located at the far end from FTR, resulting in a difference of about 4 Å for the G70−T73 helix between the cluster and the cross-linked complex. This difference explains why the former fits the PRE data whereas the latter does not.

Thus, both orientations of Trx-m found with the docking simulations suggest the need for a rearrangement from the initial complex into the cross-linked complex. Comparison of crystal structures of free FTR with the cross-linked FTR/Trx intermediate shows no structural change in the FTR backbone conformation upon Trx-m binding. However, a local structural rearrangement of side chains for several residues of FTR is evident. In the structure of free FTR, H59 and H86 protrude into the solvent. In contrast, in the cross-linked complex, a side chain rotation of H86 creates a flat surface, enabling a flip of the indole side chain of Trx-m W36. The rotation of the side chain of H59 can further remove steric hindrance, allowing a rotational movement of Trx-m to sample the best surface complementarities. Side chain rearrangement of H59 accommodates the final position of the short helix (G70−T73) of Trx-m. Interestingly, a recent spectroscopic study highlights a functional role of H86 in the protonation/deprotonation of the cluster-interacting thiol

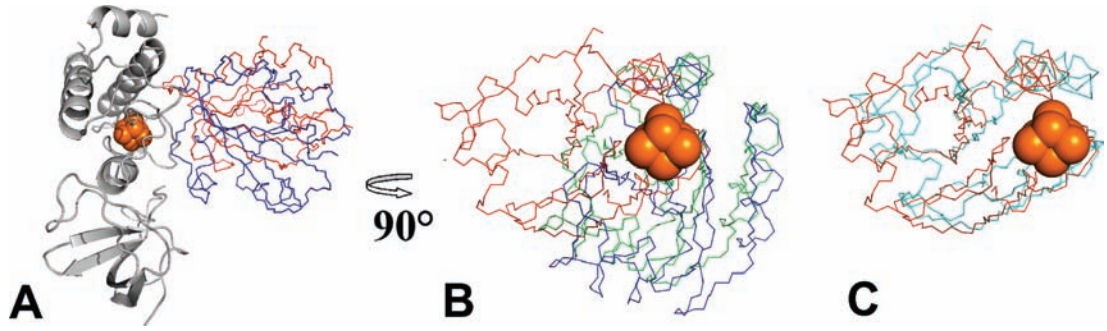

Figure 6. Structural comparisons of noncovalent and cross-linked FTR/Trx-m complexes with FTR superimposed. (A) Trx-m conformations in the noncovalent BIGGER model (blue) and cross-linked complex (red) are depicted as C^{α} traces, and FTR is shown in ribbons. The [4Fe-4S] cluster is represented as orange spheres. (B) The structures have been rotated by 90° relative to panel A and only the [4Fe-4S] cluster of FTR is shown for clarity. The HADDOCK cluster 2 model is shown as a green C^{α} trace. (C) Trx-m in the HADDOCK cluster 1 model and the cross-linked complex are shown as cyan and red C^{α} traces, respectively.

and its anchoring in close proximity of the cluster in the two-electron-reduced intermediate.[19] Previous ^{15}N relaxation measurements suggested that dynamics of loops and a tryptophan side chain of thioredoxin *E. coli* occur on various time scales.[20] Such mobility may be required for Trx to interact with other proteins for thiol−disulfide exchange. Conformational fluctuation coupled with thiol−disulfide transfer was observed for the interaction of Trx from *Bacillus subtilits* with arsenate reductase.[21] In view of these findings, we propose that upon complex formation of FTR and Trx-m, first an initial, noncovalent complex is formed that undergoes a reorientation accompanied by side-chain rearrangements to form the covalent intermediate.

Noncovalent Ternary Complex. The formation of a ternary complex of Fd with the cross-linked FTR/Trx-m complex in solution has been demonstrated by size exclusion chromatography.[22] Our NMR titration experiments show that the noncovalent binary complex formed by FTR/Trx-m can also interact with Fd to form a ternary complex. The elongated, flat structure of FTR seems optimal for simultaneous binding of its two substrates, enabling a flow of electrons from the [2Fe-2S] cluster in Fd via the [4Fe-4S] cluster of FTR to the disulfide bond in Trx.

Conclusion

The interaction of Fd, FTR, and Trx-m in an electron-transfer chain was studied by NMR. A noncovalent ternary complex was shown to form in solution. Docking models of the binary complex of Trx-m and FTR suggest a change in the orientation of the two proteins when the noncovalent binary complex reacts to form a covalent complex. This study shows that paramagnetic NMR and X-ray diffraction are complementary in the study of transient electron-transfer complexes.

Acknowledgment. P.S. thanks Prof. Dr. Jean-Marc Neuhaus for generously providing postretirement office and laboratory space. Prof. Dr. Alexandre Bonvin is acknowledged for his help with the HADDOCK web server. Support from the Chemical Sciences, Geosciences and Biosciences Division, Office of the Basic Energy Sciences, Office of Sciences, U.S. Department of Energy (Contract No. DE-FG03-99ER20346 to D.B.K.) and a grant (D-0710 to D.B.K.) from the Robert A. Welch Foundation for funding the production of the ferredoxin and thioredoxin used in this study and for portions of the experimental design and interpretation of the data is gratefully acknowledged. This project is also supported by the Netherlands Organisation for Scientific Research grant 700.52.425 (M.U.) and the Volkswagenstiftung grant I/80854 (X.F.X., M.U.). Research by P.S. was supported by the Schweizerischer Nationalfonds.

Supporting Information Available: Two tables with the HADDOCK cluster data and the Fd chemical shift perturbations, a list of experimental restraints for HADDOCK, and a figure showing the chemical shift perturbations of Fd amides upon binding to FTR and FTR-Trx. This material is available free of charge via the Internet at http://pubs.acs.org.

JA904205K

(19) Walters, E. M.; Garcia-Serres, R.; Naik, S. G.; Bourquin, F.; Glauser, D. A.; Schürmann, P.; Huynh, B. H.; Johnson, M. K. *Biochemistry* **2009**, *48*, 1016–1024.
(20) Stone, M. J.; Chandrasekhar, K.; Holmgren, A.; Wright, P. E.; Dyson, H. J. *Biochemistry* **1993**, *32*, 426–435.
(21) Li, Y.; Hu, Y. F.; Zhang, X. X.; Xu, H. M.; Lescop, E.; Xia, B.; Jin, C. W. *J. Biol. Chem.* **2007**, *282*, 11078–11083.
(22) Glauser, D. A.; Bourquin, F.; Manieri, W.; Schürmann, P. *J. Biol. Chem.* **2004**, *279*, 16662–16669.